JOURNAL OF AIRCRAFT
Vol. 32, No. 1, January–February 1995

Unsteady Ground Effects on Aerodynamic Coefficients of Finite Wings with Camber

A. O. Nuhait*
King Saud University, Riyadh 11421, Saudi Arabia

A numerical investigation on finite thin cambered wings moving near ground in unsteady flow was conducted. The numerical model is based on the general three-dimensional vortex-lattice method in which the wake is computed as part of the solution. The image technique is used to simulate the ground effects. The computed results indicate that the percentage changes in the aerodynamic coefficient (C_L and C_M) increase with proximity to the ground. The greater the sink rate, the weaker the increase, which is consistent with the trend shown by other experimental investigators for flat wings. Increasing the aspect ratio increases the ground effect, causing wings to start feeling the ground at higher positions. The ground effects are weaker as the camber ratio increases, consistent with the results of two-dimensional plates. Moving the position of maximum camber backward has a similar effect. Meanlines of NACA five-digit series showed bigger increase in C_L and C_M compared to NACA four-digit and six-digit series meanlines. Increasing the angle of attack increases the ground effects in conflict with the results of two-dimensional plates.

Nomenclature

A_{ij} = normal component of the velocity induced at the control point of element i by a unit circulation around the vortex segments enclosing element j
AR = aspect ratio
C_L, C_{L_z} = lift coefficient in and out of ground effect, respectively
C_M, C_{M_z} = pitching moment (about leading edge) in and out of ground effect, respectively
c = chord
e = camber ratio
G = circulation of each vortex ring
$H_{0.25}$ = height of the quarter-chord point above ground
$h_{0.25}$ = $H_{0.25}/c$
N = number of elements
NT = number of time steps
$\boldsymbol{n}$ = unit vector normal to the wing surface
p = position of maximum camber
$\boldsymbol{r}$ = position vector
t = time, dimensionless
$\boldsymbol{V}$ = velocity vector relative to the ground-fixed (G-F) frame of reference
V_A = linear velocity of the wing
$\boldsymbol{v}$ = velocity vector relative to the body-fixed (B-F) frame of reference
XYZ = ground-fixed coordinates, G-F
xyz = body-fixed coordinates, B-F
α = angle of attack, deg, $\gamma + \theta$
Γ = circulation of a straight vortex segment
γ = flight-path angle, deg
$\Delta C_L/C_{L_z}$ = $(C_L - C_{L_z})/C_{L_z}$
$\Delta C_M/C_{M_z}$ = $(C_M - C_{M_z})/C_{M_z}$
Δt = time increment, dimensionless
θ = pitch angle, deg

Presented as Paper 93-3423 at the AIAA 11th Applied Aerodynamics Conference, Monterey, CA, Aug. 9–11, 1993; received Dec. 30, 1993; revision received May 16, 1994; accepted for publication May 19, 1994.

*Chairman, Mechanical Engineering Department. Member AIAA.

Introduction

IT is well known that the aerodynamic forces and moments of an aircraft are influenced by the proximity to the ground. This phenomenon is called ground effect. Extensive research has been done for the past 70 yr in order to understand and predict this phenomenon. During takeoff and landing the flow is inherently unsteady, even if the aircraft is moving at constant speed. This is because the height of the aircraft above the ground changes continuously with time, which in turn, makes the bound circulation around the wing change continuously with time too, causing vorticity to be shed into the wake.

Most of previous researchers treated this unsteady flow problem in quasisteady fashion by solving the steady flow around a wing moving parallel to the ground at fixed heights above the ground. The effects of wake deformation and roll up on the aerodynamic coefficients were not included in these studies. To the author's knowledge, there are very few experimental and theoretical studies in the literature that treated this problem as unsteady flow. Moreover, these studies are limited to flat wings, while practical wings are cambered and have thickness. Full experimental parametric study of the effects of camber or thickness is difficult and expensive. Hence, it is felt that there is a place in the literature for a theoretical study on cambered thin wings moving near ground in unsteady flow. The computed results should be experimentally verified when experimental data become available.

In this article, the unsteady model presented by Nuhait and Mook[1] for flat wings is extended to study the ground effects on cambered thin wings. Specifically, the effects of camber parameters on the changes in the aerodynamic coefficients and on wake shape as the ground is approached will be quantified. The camber parameters studied are camber ratio, position of maximum camber, and shape of camber line. The study is done for different wing aspect ratios, sink rates, and angles of attack.

Previous Work

Wieselsberger[2] was apparently the first to solve the ground effect problem theoretically in 1922. He introduced the image of the real wing and its trailing vortices, thereby satisfying the no-penetration boundary condition on the ground surface automatically. The problem became similar to a biplane configuration. He used the lifting-line theory of Prandtl and the

concept of induced drag of multiplane configurations to come up with a correction that was used to modify the classical induced drag and induced angle of attack of wings out of ground effects. Wieselsberger placed the trailing vortices parallel to the ground and ignored the effect of the bound vortex in the image. As a result, the theory is limited to thin wings of large aspect ratios at small angles of attack, with small sweep-back angles, and at relatively large distances above the ground.

Since the time of Wieselsberger,[2] almost all theoretical researchers have used the method of images for modeling the ground effect and solved steady flow around wings at fixed heights above the ground (a situation that may be called "steady ground effect"), and have assigned the wake position. This steady model did not account for two important phenomena. The first is the deformation and roll up of the wake into its natural force-free position. The second is the true unsteady nature of the flow brought by vorticity shed into the wake resulting from changing height above ground, a situation that may be called "unsteady ground effect." In 1985, Chen and Schweikhard[3] solved the unsteady (dynamic) problem for a two-dimensional flat plate, assuming the wake to be straight along the flight path. Such an assumption represents an approximation whose effect was not known until recently.[4,5] Katz[6] used a vortex-lattice method allowing the wake to deform freely to solve the flow around a finite wing moving near ground as found in racing cars. Chang[7] and Chang and Muirhead[8] studied experimentally several thin, flat, delta wings in both steady and unsteady ground effects. Kemmerly et al.[9] evaluated a moving-model technique for the measurement of unsteady ground effect. Nuhait,[10] Nuhait and Mook,[1] and Mook and Nuhait[12] used the general vortex-lattice method, allowing the wake to deform freely, to study finite flat wings in unsteady ground effect. Lee et al.[11] presented experimental data for F-106B and XB-70 aircraft models in unsteady ground effect. Recently, Nuhait and Zedan[4] and Zedan and Nuhait[5] used a two-dimensional vortex-lattice method, allowing the wake to deform to its natural force-free position, to study flat and cambered plates moving near ground, respectively. Nuhait and Zedan[13] used a two-dimensional-panel method, also allowing the wake to deform to its natural force-free position, to study thick airfoils moving near ground.

Method of Approach

In the present model, we have made all variables dimensionless by using three characteristic variables: 1) the speed characterizing the motion of the wing U, the physical length of a chordwise increment of the bound lattice L, and the characteristic time (L/U). The flow considered is incompressible, inviscid, and separates only along the trailing edges and wingtips. Furthermore, the flow is assumed symmetrical about a plane passing through the midspan section of the wing. Thus, we have used half of the wing and its wake in order to reduce the computer execution time. We simulate the ground effect by adding the image of the wing and its wake below the ground, thereby making the ground a stream surface as shown in Fig. 1. Clearly, the problem of one wing and its wake flying near ground becomes as two wings with their wakes moving together while satisfying the no-penetration boundary condition, always, on the ground plane. This may appear to complicate the problem; however, in reality the problem has been simplified as will be shown later.

The problem is solved by using two coordinate systems: one fixed to the ground (G-F) and the other fixed to the wing (B-F) as shown in Fig. 1. The wing, its wake and their images are represented by sheets of vorticity. The vortex sheet representing the wing has its position specified, whereas the position of the vortex sheet representing the wake is not known in advance; it deforms freely and rolls up into its natural force-free position during the simulation. The two vortex sheets are joined along the trailing edges and wingtips. They are replaced

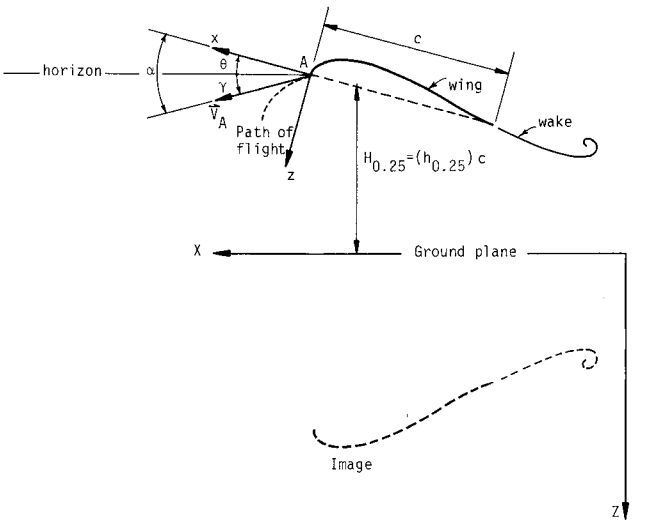

Fig. 1 Sketch of the side view of cambered wing; its wake and their images and the coordinate systems.

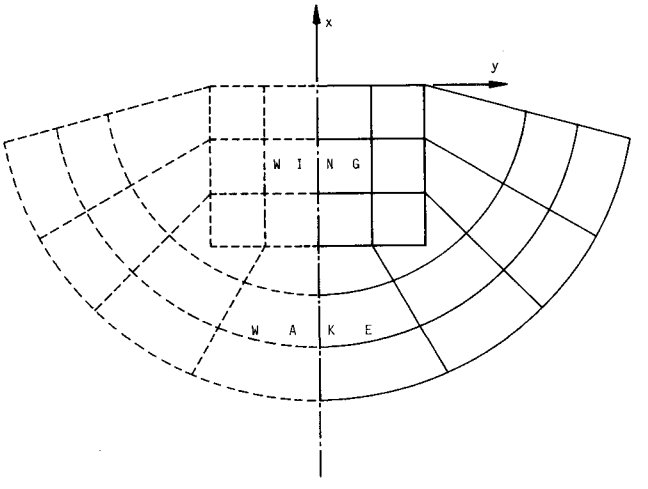

Fig. 2 Representation of the wing and its wake with a vortex lattice.

with a lattice of discrete vortex lines as shown in Fig. 2. The solid and broken lines represent discrete vortex segments for the right and left halves of the wing and their wakes, respectively. The absolute velocity induced by all vortex segments is computed by using the Biot-Savart Law. In Fig. 3, a vortex segment and its three images for symmetrical flow near ground is shown. The velocity induced at point p by the vortex segment 12 and its three images is given by the relationship:

$$V = \frac{\Gamma}{4\pi}\left\{\frac{\boldsymbol{\Omega}\times\boldsymbol{r}_1}{|\boldsymbol{\Omega}\times\boldsymbol{r}_1|^2}\left[\boldsymbol{\Omega}\cdot\left(\frac{\boldsymbol{r}_1}{|\boldsymbol{r}_1|}-\frac{\boldsymbol{r}_2}{|\boldsymbol{r}_2|}\right)\right] + \frac{\boldsymbol{\Omega}'\times\boldsymbol{r}_2'}{|\boldsymbol{\Omega}'\times\boldsymbol{r}_2'|^2}\left[\boldsymbol{\Omega}'\cdot\left(\frac{\boldsymbol{r}_2'}{|\boldsymbol{r}_2'|}-\frac{\boldsymbol{r}_1'}{|\boldsymbol{r}_1'|}\right)\right] - \frac{\boldsymbol{\Omega}''\times\boldsymbol{r}_1''}{|\boldsymbol{\Omega}''\times\boldsymbol{r}_1''|^2}\left[\boldsymbol{\Omega}''\cdot\left(\frac{\boldsymbol{r}_1''}{|\boldsymbol{r}_1''|}-\frac{\boldsymbol{r}_2''}{|\boldsymbol{r}_2|}\right)\right] - \frac{\boldsymbol{\Omega}'''\times\boldsymbol{r}_2'''}{|\boldsymbol{\Omega}'''\times\boldsymbol{r}_2'''|^2}\left[\boldsymbol{\Omega}'''\cdot\left(\frac{\boldsymbol{r}_2'''}{|\boldsymbol{r}_2'''|}-\frac{\boldsymbol{r}_1'''}{|\boldsymbol{r}_1'''|}\right)\right]\right\} \tag{1}$$

where $\boldsymbol{r}_1$ and $\boldsymbol{r}_2$ are the position vectors from points 1 and 2 to point p, respectively. $\boldsymbol{\Omega}$ is the position vector from points 1 to 2 ($\boldsymbol{\Omega} = \boldsymbol{r}_2 - \boldsymbol{r}_1$). Γ is the circulation around the vortex segment. The superscripts ′, ″, ‴ denote the three images as shown in the figure.

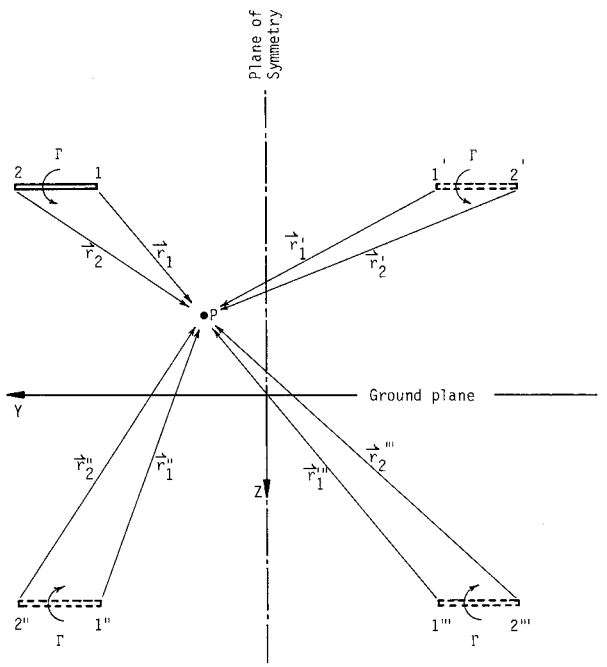

Fig. 3 Vortex segment and its three images for symmetrical flow.

The total velocity field induced by all the vortex segments must satisfy the continuity equation and the following seven conditions: 1) $V_{\text{disturbance}} \rightarrow 0$ at infinity, 2) the normal-velocity component on the ground is zero, 3) the normal-velocity component on the wing plane of symmetry ($Y = 0$) is zero, 4) spatial conservation of circulation, 5) the pressure is continuous in the wake, 6) the so-called unsteady Kutta condition is satisfied along the trailing edges and wingtips, and finally 7) the no-penetration boundary condition is satisfied on the wing surface. It was stated previously that the velocity induced by all the vortex segments is computed using the Biot-Savart law [Eq. (1)]. Hence, the continuity equation and the first condition are satisfied automatically. Clearly, from Eq. (1), the second and third conditions are satisfied too because of symmetry with respect to the ground and to the wing plane of symmetry. The fourth condition (spatial conservation of circulation) is satisfied by taking the circulation to be the same for all the discrete vortex segments of the same loop. The fifth condition (no pressure jump across the wake) is satisfied by convecting the wake at the local fluid particle velocity [thus enforcing the condition $(D\Gamma/Dt) = 0$, which leads to a temporal conservation of circulation]. The sixth condition is satisfied by shedding all vorticity generated at the trailing edges and wingtips. The seventh condition (no-penetration boundary condition) is written simply as

$$[(\boldsymbol{V} - \boldsymbol{V}_A)\cdot\boldsymbol{n}]_{\text{on the wing surface}} = 0 \tag{2}$$

where $\boldsymbol{V}$ is the velocity of the fluid particle. $\boldsymbol{V}_A$ is the velocity of the moving frame of reference (point A) that is attached to the wing (see Fig. 1).

The wing is divided into a finite number of elements N. In Fig. 4, the right half of a cambered wing is shown. Each element consists of four vortex segments. In the figure, the wing is moving toward the top of the page. The no-penetration boundary condition is imposed at one "control point" on each element located at its centroid. At the start of motion (impulsive start, no wake yet exists), the no-penetration boundary condition [Eq. (2)] becomes

$$\sum_{j=1}^{N} A_{ij}G_j = (\boldsymbol{V}_A\cdot\boldsymbol{n})_i \quad \text{for} \quad i = 1, 2, 3, \ldots, N \tag{3}$$

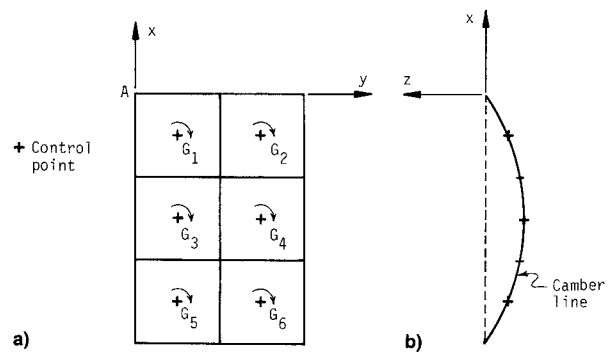

Fig. 4 Discretization of the cambered wing (right half): a) top and b) side view.

where A_{ij} is normal component of velocity at the control point of element i induced by unit circulation around the four vortex segments enclosing element j (vortex ring) and its three images. G_j is the circulation around the vortex segments enclosing element j. As a result of nonzero γ (see Fig. 1), A_{ij} is recomputed at each time step.

At the beginning of the first time step, $NT = 1$, all the circulations in the bound and free portions of the vortex lattice are zero. At the end of the first time step, the circulations in the bound portion have changed [after solving Eq. (3)], and a vortex line is generated along the trailing edges and wingtips (starting vortex dictated by the requirement of spatial conservation of circulation). At the beginning of the second time step ($NT = 2$), and in order to satisfy the unsteady Kutta condition, all the vorticity formed along the sharp edges is shed and convected downstream at the local fluid particle velocity in order to ensure that pressure is continuous in the wake. The local fluid particle velocity $\boldsymbol{v}$ is given by

$$\boldsymbol{v} = \boldsymbol{V} - \boldsymbol{V}_A \tag{4}$$

where $\boldsymbol{V}$ is the absolute velocity induced by all vortex segments and their images computed by using Eq. (1). The circulation of the shed vortex at the new position is kept the same as at the old position in order to guarantee the temporal conservation of circulation. In order to guarantee the spatial conservation of circulation, the starting vortices at the old and new positions are joined at the nodal points with connectors. The new position of the node k, $\boldsymbol{r}_k(t + \Delta t)$, is computed according to the following formula:

$$\boldsymbol{r}_k(t + \Delta t) = \boldsymbol{r}_k(t) + [\boldsymbol{v}_k(t)]\Delta t \tag{5}$$

in which $\boldsymbol{v}_k(t)$ is computed by using Eq. (4). The wake is created as a result of shedding and convecting the trailing edge and the wingtip (starting) vortices. Including the effects of the wake and its three images, the no-penetration boundary condition of Eq. (2) becomes

$$\sum_{j=1}^{N} A_{ij}G_j = [(\boldsymbol{V}_A - \boldsymbol{V}_W)\cdot\boldsymbol{n}]_i \quad \text{at} \quad i = 1, 2, 3, \ldots, N \tag{6}$$

where $\boldsymbol{V}_W$ is the velocity induced by the wake and its three images whose position and vorticity are known. At the end of the second time step, the bound circulations are recomputed by solving Eq. (6). A second "starting" vortex forms along the sharp edges. At the beginning of the third time step ($NT = 3$), the second starting vortex is shed and convected downstream to its new position as required by the unsteady Kutta condition. Simultaneously, the first starting vortex is convected to a new position. The wake grows as a result of shedding and convecting vortices. The procedure for finding the solution of Eq. (6) can be repeated for any desired number of time steps.

The aerodynamic forces and moments are computed by integrating the pressure-jump distribution over the wing. The

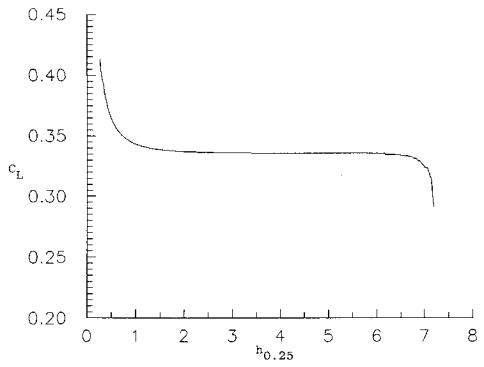

Fig. 5 Unsteady ground effect on C_L of a cambered wing approaching ground from impulsive start; circular-arc mean line with $e = 0.03$, $AR = 1$, $\gamma = 10$ deg, and $\alpha = 6$ deg.

pressure jump across each element is found at the control point of that element by using the unsteady Bernoulli equation as described in Ref. 10.

Results and Discussion

The present aerodynamic model was programmed in Fortran and run on the IBM 370 3083 JX mainframe computer. γ is referred to as the sink rate V_{AZ} (Fig. 1). They are interrelated through the relation

$$\gamma = \tan^{-1}(V_{AZ}/V_{AX}) \tag{7}$$

In this article the wing moves along a straight line (i.e., γ = const). The dimensionless time step Δt was taken to be unity. This yields lengths between vortex segments in the wake that are about the same as those on the wing. According to the present model, the number of vortex segments shed and convected into the wake is equal to the number of time steps NT. This will increase the computer execution time tremendously. One way to reduce the execution time is to neglect the effect of wake vortex segments when they are far enough from the wing. This was implemented by truncating the wake when the number of vortex segments reaches a certain number. Beyond this number the solution is marched in time neglecting the effects of early shed vortex segments assuming they are far enough. A vortex segment located at a position six chord lengths behind the wing trailing edge was determined to be far enough. In a typical run in which the wing starts moving at $h_{0.25} = 7.2$ with $\gamma = 10$ deg, NT needed to reach ground is 400, and the execution time is about 32 h. For $\gamma = 2.5$ deg, the execution time is quite higher.

During the simulation, the wing is set in motion impulsively. To filter out the unsteady effect due to this impulsive start, the wing motion is started at a position too far to feel the ground. The flow is allowed to reach steady conditions before the wing enters the ground effects. As the wing approaches the ground, the circulation around it changes with time (height), making the flow unsteady. Numerical results of a typical run are shown in Fig. 5 in which three distinct regions are shown. The first region C_L increases as the wing starts to move reaching an asymptotic value in the second region as the flow reaches steady conditions. The last region shows the increase of C_L due to the unsteady ground effects only. The presented results are confined to the third region (unsteady ground effects).

Effect of Sink Rate

To investigate this effect, a cambered wing with circular-arc mean line is used. The camber ratio and angle of attack are 0.03 and 6 deg, respectively. The wing aspect ratio is unity. The sink rate is varied by varying γ. In Figs. 6a and 6b, the percentage changes in C_L and C_M as functions of height of the quarter-chord point above the ground ($h_{0.25}$) are shown for different γ. It is obvious that C_L and C_M increase as the

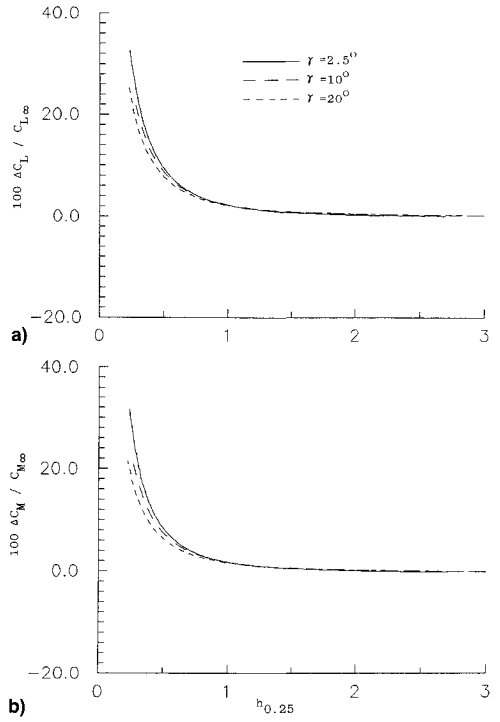

Fig. 6 Deviation of a) C_L and b) C_M as functions of height above ground for cambered wing at different sink rates; circular-arc mean line with $e = 0.03$, $AR = 1$, and $\alpha = 6$ deg.

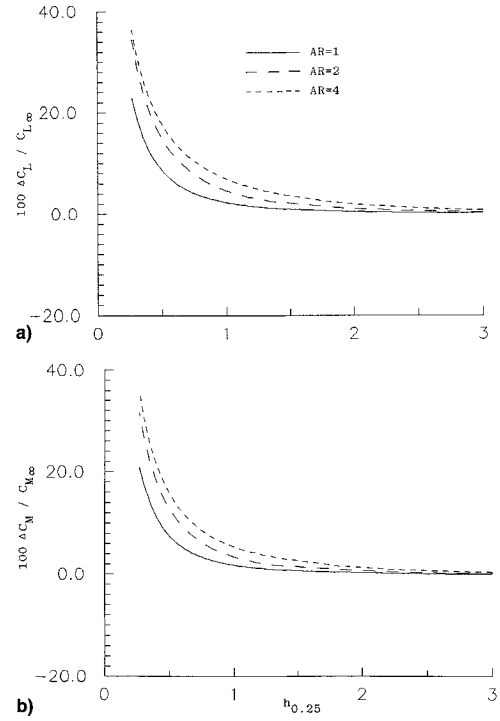

Fig. 7 Deviation of a) C_L and b) C_M as functions of height above ground for cambered wing with different aspect ratios; circular-arc mean line with $e = 0.03$, $\gamma = 10$ deg, and $\alpha = 6$ deg.

wing approaches the ground. The higher the sink rate, the lower the effect that contradicts the two-dimensional circular-arc plate results.[5] This is attributed to the three-dimensional effects. These results are consistent with the trend reported in a number of experimental investigations.[7-9,11]

Effect of Aspect Ratio

To study this effect, three wings with a circular-arc mean line are used. All three wings have identical camber ratio e

= 0.03, moving at the same sink rate γ = 10 deg, and at the same angle of attack α = 6 deg. Figures 7a and 7b show plots of the percentage changes in C_L and C_M as a function of height of the quarter-chord point above the ground for different aspect ratios. It is clear that the ground effects increase the aerodynamic coefficients, and that these effects are stronger for larger aspect ratios. A wing with a larger aspect ratio starts feeling the ground at a higher level.

Effect of Camber Ratio

Two wings with circular-arc mean line are used. These wings have a identical aspect ratio of 1, move with identical sink rate of 10 deg, and at angle of attack of 6 deg. The camber ratios are 0.03 and 0.06. In Figs. 8a and 8b, the percentage changes in C_L and C_M as functions of $h_{0.25}$ are shown for these two camber ratios and for a flat wing (e = 0). The ground effects increase C_L and C_M, the increase is weaker for higher camber ratios. This trend is consistent with the results of two-dimensional circular-arc plates.[5]

Actual computed wakes of cambered (e = 0.03) and flat (e = 0) wings in unsteady flow are shown in Figs. 9 and 10 in the G-F frame of reference. These wings have identical aspect ratios of 1, move with identical sink rates of 2.5 deg, and at an angle of attack of 6 deg. The side views are shown in Fig. 9, whereas the top views are presented in Fig. 10. Note that the scales in the two figures are different. The case of

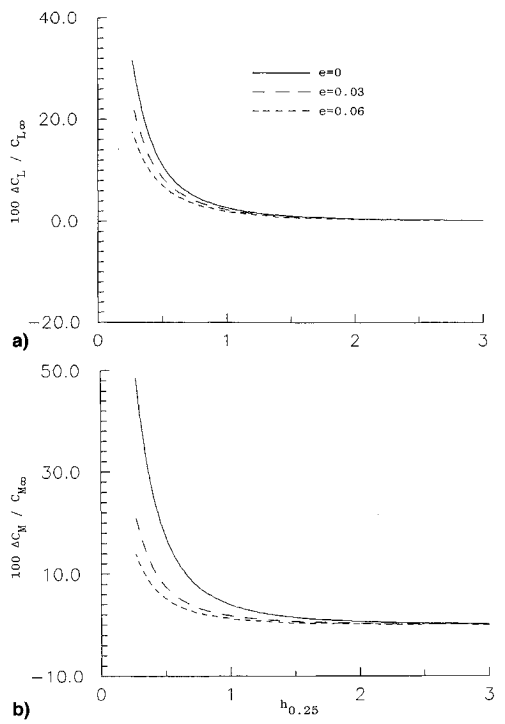

Fig. 8 Deviation of a) C_L and b) C_M as functions of height above ground for cambered wing with different camber ratios; circular-arc mean line, AR = 1, γ = 10 deg, and α = 6 deg.

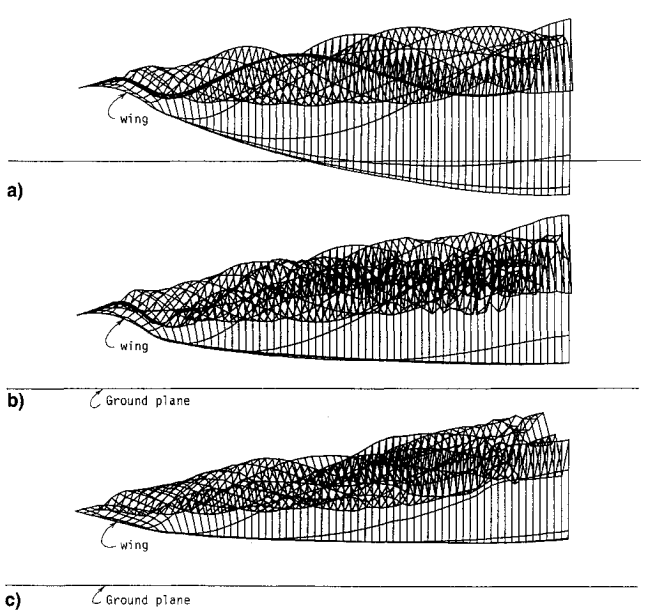

Fig. 9 Side views of actual computed wakes of two wings in unsteady flow: a) cambered wing (e = 0.03) out of ground effect ($h_{0.25}$ = 1.90), b) cambered wing (e = 0.03) in ground effect ($h_{0.25}$ = 0.24), and c) flat wing (e = 0) in ground effect ($h_{0.25}$ = 0.24); AR = 1, γ = 2.5 deg, and α = 6 deg.

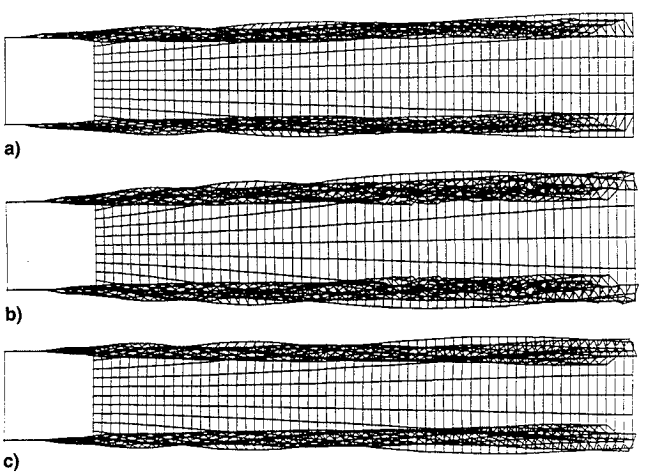

Fig. 10 Top views of actual computed wakes of two wings in unsteady flow: a) cambered wing (e = 0.03) out of ground effect ($h_{0.25}$ = 1.90), b) cambered wing (e = 0.03) in ground effect ($h_{0.25}$ = 0.24), and c) flat wing (e = 0) in ground effect ($h_{0.25}$ = 0.24); AR = 1, γ = 2.5 deg, and α = 6 deg.

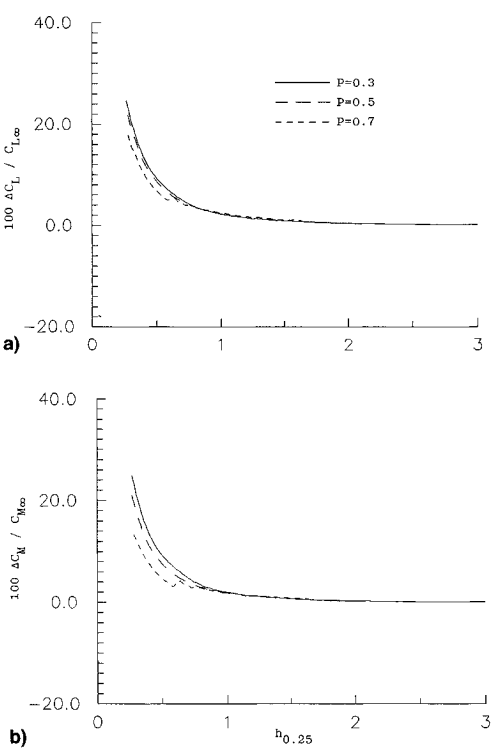

Fig. 11 Deviation of a) C_L and b) C_M as functions of height above ground for cambered wing with different locations of maximum camber; NACA four-digit series mean line with e = 0.03, AR = 1, γ = 10 deg, α = 6 deg.

the cambered wing out of ground effect ($h_{0.25} = 1.90$) is shown in part a) of both figures. The near ground case ($h_{0.25} = 0.24$) is shown in parts b) and c) of both figures for cambered and flat wings, respectively. The position of the ground plane is shown in parts b) and c) of Fig. 9, it is also included in part a) for comparison. Clearly, the effect of ground is to restrict the downward movement of the wake, causing it to spread. The wake position (side view) is lower for the case of the wing with camber near ground compared to the flat wing.

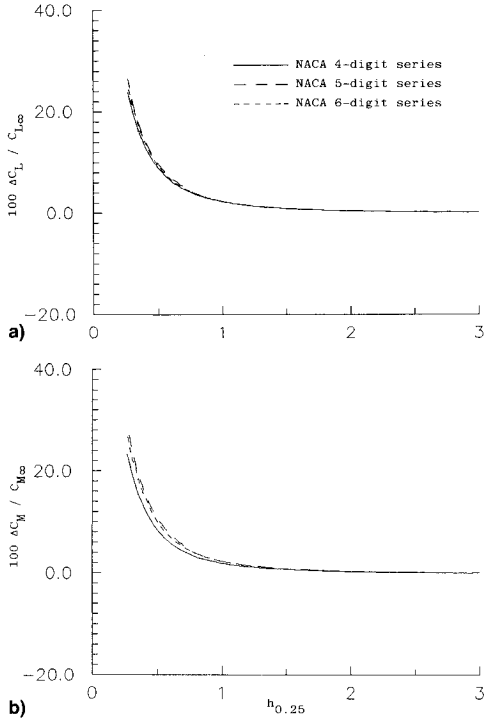

Fig. 12 Deviation of a) C_L and b) C_M as functions of height above ground for cambered wing with different mean line shapes; $e = 0.0325$, $p = 0.325$, $AR = 1$, $\gamma = 10$ deg, and $\alpha = 6$ deg.

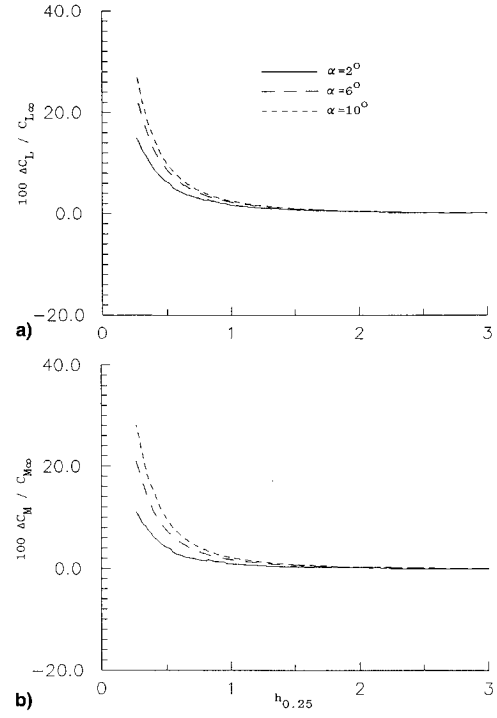

Fig. 13 Deviation of a) C_L and b) C_M as functions of height above ground for cambered wing at different angles of attack; circular-arc mean line with $e = 0.03$, $AR = 1$, and $\gamma = 10$ deg.

Effect of Position of Maximum Camber

To study this effect, the mean line of the NACA four-digit series airfoil is used. The camber ratio is fixed at 0.03 while p is varied. The angle of attack and sink rate are taken to be 6 and 10 deg, respectively. In Figs. 11a and 11b, variation of $\Delta C_L/C_{L_\alpha}$ and $\Delta C_M/C_{M_\alpha}$ are shown for wings with different p approaching ground. Clearly, the ground effect increases the coefficients. The farther back the position of maximum camber, the lower the ground effects.

Effect of Camberline Shape

The results are compared for three camber lines with identical camber ratio and identical position of maximum camber, but with different geometry (shape). The camber lines chosen have $e = 0.0325$ and $p = 0.325$; one of them is the mean line for the NACA four-digit series, the second is the mean line for the NACA five-digit series, and the third is the mean line for the NACA six-digit series. The angle of attack and sink rate are fixed at 6 and 10 deg, respectively. The results in Fig. 12 indicate that the increase in C_L as the ground is approached is slightly greater for the five-digit family mean line. The results for $\Delta C_M/C_{M_\alpha}$ show more appreciable differences than for $\Delta C_L/C_{L_\alpha}$.

Effect of Angle of Attack

To study this effect, a cambered wing with a circular-arc mean line with $e = 0.03$ is used. α was varied while γ was fixed at 10 deg. The results are shown in Fig. 13. Clearly, the ground effect increases the aerodynamic coefficients with greater increase for larger angles of attack. This is in slight contrast with results of the two-dimensional plates,[5] where the increase in the aerodynamic coefficients is lower at higher angles of attack. This difference in behavior may be attributed to the three-dimensional effects in the present case.

Summary and Conclusions

The unsteady model presented by Nuhait and Mook,[1] which is based on the general three-dimensional vortex-lattice method, was extended to study finite cambered wings moving near ground. The ground effects are simulated by the method of images, whereas the wake vorticity and position are computed as part of the solution. During the numerical simulation, wings are set in motion impulsively far from ground and the flow is allowed to reach steady conditions before wings start feeling ground. The sink rate was varied through varying the flight-path angle. The effects of camber ratio, aspect ratio, sink rate, position of maximum camber, angle of attack, and camber line shape on the changes in C_L, C_M, and wake shape as the ground is approached were quantified through systematic investigation. In general, the computed results indicate that the percentage changes in C_L and C_M increase with proximity to ground. The greater the sink rate, the weaker the increase, this is consistent with the trend shown by other experimental investigators.[7-9,11] Increasing the aspect ratio increases ground effect causing wings to start feeling the ground at higher positions. The ground effects are weaker as the camber ratio increases consistent with the results of two-dimensional plates.[5] Moving the position of maximum camber backward has a similar effect. Mean lines of the NACA five-digit series showed a bigger increase in C_L and C_M compared to NACA four-digit and six-digit series mean lines. Increasing the angle of attack increases the effect of ground opposite to the results of two-dimensional plate.[5]

Acknowledgment

The author wishes to thank the staff of King Saud University Computer Center for their cooperation and help.

References

[1]Nuhait, A. O., and Mook, D. T., "Numerical Simulation of Wings in Steady and Unsteady Ground Effects," *Journal of Aircraft*, Vol. 26, No. 6, 1989, pp. 1081–1089.

[2]Wieselsberger, C., "Wing Resistance Near Ground," NACA TM 77, April 1922.

[3]Chen, Y.-S., and Schweikhard, W. G., "Dynamic Ground Effects on a Two-Dimensional Flat Plate," *Journal of Aircraft*, Vol. 22, No. 7, 1985, pp. 638–640.

[4]Nuhait, A. O., and Zedan, M. F., "Numerical Simulation of Unsteady Flow Induced by a Flat Plate Moving Near Ground," *Journal of Aircraft*, Vol. 30, No. 5, 1993, pp. 611–617.

[5]Zedan, M. F., and Nuhait, A. O., "Unsteady Effect of Camber on Aerodynamic Characteristics of a Thin Airfoil Moving Near Ground," *Aeronautical Journal of the Royal Aeronautical Society*, Vol. 96, No. 959, 1992, pp. 343–350.

[6]Katz, J., "Calculation of the Aerodynamic Forces on Automotive Lifting Surfaces," *Journal of Fluids Engineering*, Vol. 107, Dec. 1985, pp. 438–443.

[7]Chang, R. C., "An Experimental Investigation of Dynamic Ground Effect," Ph.D. Dissertation, Dept. of Aerospace Engineering, Univ. of Kansas, Lawrence, KS, April 1985.

[8]Chang, R. C., and Muirhead, V. U., "Effect of Sink Rate on Ground Effect of Low-Aspect-Ratio Wings," *Journal of Aircraft*, Vol. 24, No. 3, 1987, pp. 176–180.

[9]Kemmerly, G. T., Paulson, J. W., and Compton, M., "Exploratory Evaluation of Moving-Model Technique for Measurement of Dynamic Ground Effects," *Journal of Aircraft*, Vol. 25, No. 6, 1988, pp. 557–562.

[10]Nuhait, A. O., "Numerical Simulation of Feedback Control of Aerodynamic Configurations in Steady and Unsteady Ground Effects," Ph.D. Dissertation, Dept. of Engineering Science and Mechanics, Virginia Polytechnic Inst. and State Univ., Blacksburg, VA, Oct. 1988.

[11]Lee, P.-H., Lan, C. E., and Muirhead, V. U., "Experimental Investigation of Dynamic Ground Effect," *Journal of Aircraft*, Vol. 26, No. 6, 1989, pp. 497, 498.

[12]Mook, D. T., and Nuhait, A. O., "Simulation of the Interaction Between Aerodynamics and Vehicle Dynamics in General Unsteady Ground Effect," AIAA Paper 89-1498, June 1989.

[13]Nuhait, A. O., and Zedan, M. F., "Unsteady Grounds Effects on Aerodynamic Coefficients of Thick Airfoils," *Arabian Journal for Science and Engineering* (to be published).